Stability of some stationary solutions to the forced KdV equation with one or two bumps

**Frédéric Chardard · Frédéric Dias ·
Hai Yen Nguyen · Jean-Marc Vanden-Broeck**

Abstract   Free-surface flows past submerged obstacles in a channel are considered. The fluid is assumed to be inviscid and incompressible and the flow to be irrotational. The first-order approximation of long nonlinear surface waves over one or two bumps results in a forced Korteweg–de Vries (fKdV) equation. Solutions of the stationary fKdV equation are constructed and their stability is studied, either analytically or numerically. These various solutions include solitary waves over a single bump, solitary waves with two humps over a double bump, table-top solutions over a double bump and fronts.

F. Chardard
UMPA, ENS Lyon (site Sciences), 46 allée d'Italie, 69364 Lyon Cedex 07, France
e-mail: frederic.chardard@umpa.ens-lyon.fr

F. Dias (✉)
CMLA, ENS Cachan, CNRS, PRES UniverSud, 61 Av. President Wilson, 94230 Cachan, France
e-mail: frederic.dias@cmla.ens-cachan.fr

F. Dias
School of Mathematical Sciences, University College Dublin, Belfield, Dublin 4, Ireland

H. Y. Nguyen
Laboratoire de Physique des Océans, IFREMER, BP 70, 29280 Plouzané, France
e-mail: hynguyen@ifremer.fr

J.-M. Vanden-Broeck
Department of Mathematics, University College London, London, WC1E 6BT, UK
e-mail: broeck@math.ucl.ac.uk

1 Introduction

The question of flow over topography with nonlinearity and dispersion included is an intriguing one, which is reviewed for example in the book by Baines [1, Sect. 2.6]. Indeed, a forcing disturbance moving steadily in a channel can generate a variety of interesting flows. With two disturbances, the set of possible flows is even larger. Here we take a frame of reference moving with the disturbance(s). In the case of two disturbances, they are assumed to move at the same speed. Let a be a typical wave amplitude, λ a typical wavelength, h_0 the water depth in the channel away from the obstacle(s), U the speed of the moving disturbance(s) and b the height of the obstacle(s).[1] Let us also introduce the Froude number $F = U/c_0$, where $c_0 = \sqrt{gh_0}$. The fluid is assumed to be inviscid and incompressible and the flow to be irrotational. When a/h_0, $(h_0/\lambda)^2$, $F - 1$ and b/h_0 are all comparably small, a good model for the study of flows over topography is the forced Korteweg–de Vries (fKdV) equation. The literature on this subject is so vast that it is not possible to give here a full account. In what follows we have selected only a few samples of the literature. The fKdV equation has been formally derived for forcing by a moving pressure pattern by Akylas [2], and for forcing by topography in more general stratification by Grimshaw and Smyth [3]. Patoine and Warn [4] used the fKdV equation in the context of the interaction of long, quasi-stationary, baroclinic waves with topography. Pratt [5] used the fKdV equation to explain some experiments related to atmospheric flow over mountains. The fKdV equation was then used by Wu [6] to explore the basic mechanism underlying the generation of upstream advancing solitons by moving disturbances. Shen [7] studied steady solutions of a fKdV equation for channels of arbitrary cross section. Camassa and Wu [8,9] performed a stability analysis of forced steady solitary-wave solutions and confirmed their analytical findings with accurate numerical simulations. Gong and Shen [10] explored various solitary-wave solutions of the fKdV equation under several types of forcing, including a two semi-elliptic bump forcing. Shen et al. [11] investigated soliton collisions governed by the fKdV equation. In the case of a single obstacle, Dias and Vanden-Broeck [12] found new solutions called generalised hydraulic falls. These solutions are characterized by a supercritical flow on one side of the obstacle and a train of waves on the other. However, in the case of a single submerged bump, the generalised hydraulic falls are unphysical because the waves do not satisfy the radiation condition. Dias and Vanden-Broeck [13] computed new stationary solutions for the flow past two obstacles of arbitrary shape. These solutions are characterised by a train of waves 'trapped' between the obstacles. It was shown that the generalised hydraulic falls of Dias and Vanden-Broeck [12] describe locally the flow over one of the two obstacles when the distance between the two obstacles is large. Binder, Vanden-Broeck and Dias [14] compared solutions of the fKdV equation with potential flow solutions for the flow past multiple obstacles. Donahue and Shen [15] investigated numerically the stability of the hydraulic fall and cnoidal–wave solutions of the fKdV equation.

Maleewong et al. [16] added surface-tension effects to the fKdV equation and investigated steady solutions. Subsequently Grimshaw et al. [17] examined the stability of these steady solutions.

The main goal of the present paper is to review first the stability of the supercritical solitary-wave and hydraulic-fall solutions in the presence of a single obstacle, in the framework of the fKdV equation. Then new results are presented for two obstacles lying at the bottom, in particular for table-top-like solutions. Results of a novel analysis of the stability problem are confirmed by integrating numerically the fKdV equation. In Sect. 2, we introduce the fKdV equation as well as its Hamiltonian structure, which will be useful for the stability results of Sect. 6. In Sect. 3, we derive exact steady solitary-wave solutions of the fKdV equation with a single obstacle by using an inverse method. Inverse methods have a long history in hydrodynamics. Although equivalent methods have been rediscovered many times since, the first statement of the method appears to be due to Sautreaux [18]. The technique is described for example in [19, pp. 736–740]. E. O. Tuck himself used this technique in a number of publications; see [20] for a detailed account. After constructing the exact solutions, we review known stability results. Section 4 deals with hydraulic-fall solutions, again in the presence of a single obstacle. The same inverse technique leads to exact solutions. Their stability is studied numerically. In Sect. 5, we derive exact steady solitary-wave solutions with

---

[1] In the case of two obstacles, there is some arbitrariness in this choice. In fact, we implicitly make the assumption that the ratio of obstacle heights is neither too small nor too large, without going into mathematical details.

two humps in the presence of two bottom-mounted obstacles by using the same inverse method. Again we study their stability numerically. In Sect. 6, new exact table-top solutions are constructed in the presence of two obstacles. A novel theoretical analysis allows one to predict stability or instability for two special cases. The analytical results are confirmed numerically. Finally, a conclusion and discussion section is provided at the end of the paper.

2 The forced Korteweg–de Vries (fKdV) model

The classical KdV equation, which includes both nonlinearity and dispersion, can be extended to admit arbitrary forcing functions if the forcing disturbances are limited to unidirectional motion, say

$$B^* = B^*(x^* + Ut^*), \tag{2.1}$$

representing a left-going (or right-going) bathymetry when U is positive (or negative). These forcing functions are supposed to be sufficiently smooth, localized and to vanish identically for time $t^* < 0$. In the derivation of KdV-type equations, it is also assumed that the velocity U is close to critical so that $F - 1 = O(\epsilon)$. The small number ϵ is usually defined as the square of the ratio between the undisturbed water depth h_0 and a typical wavelength λ. One also requires both the ratio between wave amplitude and h_0 and the ratio between the height of the disturbance and h_0 to be $O(\epsilon)$. Then stretched coordinates are introduced and asymptotic expansions are assumed. More or less rigorous derivations of the fKdV equation can be found in several papers. Here we mention three papers: [21–23]. Shen [22] noted that quite surprisingly the range of validity of the stationary fKdV equation is not restricted to small bumps and small amplitudes! After a few substitutions and integrations, as well as a switch to dimensionless variables, one obtains the following fKdV equation as a model for open-channel flow past obstructions:

$$\eta_t = \frac{1}{6}\eta_{xxx} + \frac{3}{4}\left(\eta^2\right)_x - (F-1)\eta_x + \frac{1}{2}B_x, \tag{2.2}$$

where B is the dimensionless forcing term. The link between the physical variables and the variables appearing in the fKdV model is (∗ are used for the physical quantities):

$$x = \frac{x^* + Ut^*}{h_0}, \quad \eta = \frac{\eta^*}{h_0}, \quad B = \frac{B^*}{h_0}, \quad t = \frac{c_0 t^*}{h_0}.$$

The fKdV equation (2.2) has a Hamiltonian structure. This structure was used for example by Camassa and Wu [9] to investigate nonlinear stability properties. The fKdV equation can indeed be written as

$$\eta_t = \frac{\partial}{\partial x}\frac{\delta\mathcal{H}}{\delta\eta}, \tag{2.3}$$

where $\mathcal{H}$ is the Hamiltonian:

$$\mathcal{H}(\eta) = \frac{1}{6}\int_{\mathbb{R}}\left(-\frac{1}{2}\eta_x^2 + \frac{3}{2}\eta^3 - 3(F-1)\eta^2 + 3B\eta\right)dx. \tag{2.4}$$

One takes $\langle u, v \rangle \rightarrow \int_{\mathbb{R}} uv$ as scalar product.

When one linearizes (2.3) near a stationary solution, $\widetilde{\eta}$, one obtains

$$\eta_t = \frac{\partial}{\partial x}\mathcal{L}\eta,$$

where $\mathcal{L}$ is the Hessian of the functional $\mathcal{H}$:

$$\mathcal{L}\eta = \left[\frac{\delta^2\mathcal{H}}{\delta\eta^2}\right]_{\eta=\widetilde{\eta}}(\eta) = \frac{1}{6}\left(\eta_{xx} + 9\widetilde{\eta}\eta - 6(F-1)\eta\right).$$

The linear spectral problem $\mathcal{L}\eta = \lambda\eta$ can be written as a first-order linear system:

$$\mathcal{J}U_x(x) = \mathbf{C}(x, \lambda)U(x), \quad U(x) = \begin{pmatrix}\eta \\ \eta_x\end{pmatrix}, \quad \mathcal{J} = \begin{pmatrix}0 & 1 \\ -1 & 0\end{pmatrix},$$

$$\mathbf{C}(x, \lambda) = \begin{pmatrix}6(F-1) - 9\widetilde{\eta} + 6\lambda & 0 \\ 0 & -1\end{pmatrix}. \tag{2.5}$$

Let $\sigma(\mathcal{L})$ denote the spectrum of $\mathcal{L}$. Assume that $0 \notin \sigma(\mathcal{L})$ and that the stationary solution $\widetilde{\eta}$ is symmetric (this implies that the bottom is symmetric). Then, according to Chugunova and Pelinovsky [24], the following relationship between the number of eigenmodes of $\mathcal{L}$ and those of $\partial_x \mathcal{L}$ holds:

$$n_+ = N_{\text{unst}} + N_{\text{imag}}^+, \tag{2.6}$$

where n_+ is the number of strictly positive eigenvalues of $\mathcal{L}$, N_{unst} is the number of unstable modes of $\partial_x \mathcal{L}$ and N_{imag}^+ is the number of imaginary eigenvalues of $\partial_x \mathcal{L}$ with multiplicities associated with eigenvector u such that $\langle u, \mathcal{L}u \rangle > 0$.

Note that Chugunova and Pelinovsky [24] only consider the case of a flat bottom. Since the stationary solution is assumed to be symmetric, the proof can be extended to the case with obstacles. The kernel of $\partial_x \mathcal{L}$ is now empty and there is no need to take into account the generalized kernel of $\partial_x \mathcal{L}$. More details can be found in [25].

3 One obstacle: review of localised solutions and their stability

In this section we derive exact steady solutions of the fKdV Eq. (2.2) by using an inverse method. Since this technique has been used by several authors, this section is simply a review of known results. One prescribes the profile of the free surface and then calculates the corresponding shape of the bottom. Only supercritical flows with $F > 1$ are considered.

Assume that the wave at the surface of the channel is of the form

$$\eta = A \operatorname{sech}^2 \beta x. \tag{3.7}$$

One looks for a corresponding localized bump at the bottom. In order to do this, one substitutes (3.7) in (2.2) and integrates once, assuming that the bathymetry vanishes at infinity:

$$B(x) = \frac{1}{3}\left(6(F-1)\eta - \frac{9}{2}\eta^2 - \eta_{xx}\right). \tag{3.8}$$

This expression can be written explicitly as

$$B(x) = \frac{A}{6}\left(\frac{12F - 12 - 8\beta^2}{\cosh^2 \beta x} + \frac{12\beta^2 - 9A}{\cosh^4 \beta x}\right). \tag{3.9}$$

The bottom, which is symmetric, is a linear combination of two localized bumps, one with a sech^2 behavior and the other one with a sech^4 behavior. As long as both coefficients in the linear combination are positive, the bottom will be a localized bump, of maximum amplitude G obtained at $x = 0$ and equal to the sum of both coefficients. If one fixes the maximum amplitude G, there is an infinity of choices for the parameters. There are two obvious possibilities: (i) either to take the coefficient of the sech^2 bump to be G and the other one to be zero; (ii) or to take the coefficient of the sech^4 bump to be G and the other one to be zero. These two possibilities lead to two systems of two equations:

$$\begin{cases} A\left(12F - 12 - 8\beta^2\right) = 6G \\ A\left(4\beta^2 - 3A\right) = 0 \end{cases}, \quad \begin{cases} A\left(12F - 12 - 8\beta^2\right) = 0 \\ A\left(4\beta^2 - 3A\right) = 2G \end{cases}. \tag{3.10}$$

Assuming that F and G are fixed, one finds in each case two values for the amplitude A and the corresponding value for β:

$$\begin{cases} A = F - 1 \pm \sqrt{(F-1)^2 - G} \\ \beta = \sqrt{\frac{3A}{4}} \end{cases}, \quad \begin{cases} A = F - 1 \pm \sqrt{(F-1)^2 - \frac{2G}{3}} \\ \beta = \sqrt{\frac{3}{2}(F-1)} \end{cases}, \tag{3.11}$$

as long as the Froude number is larger than the minimum value

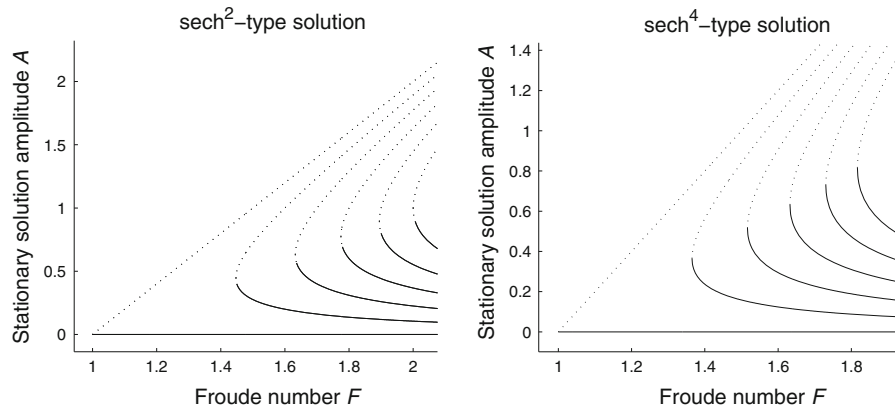$$F_{\text{min}} = 1 + \sqrt{G}, \quad F_{\text{min}} = 1 + \sqrt{\frac{2G}{3}}. \tag{3.12}$$

Fig. 1 Branches of exact steady solutions of the stationary fKdV equation in the amplitude vs. Froude number plane, when there is a single obstacle at the bottom. *Left* sech^2 bump; *Right* sech^4 bump. The *solid lines* indicate stability, the *dashed lines* instability

Note that for the sech^4 bump the coefficient β does not depend on the wave amplitude A.

The bifurcation diagram that one obtains is well-known. A detailed mathematical description is provided by Shen [7]. One obtains two branches of solutions: a perturbation of a uniform flow (with the minus sign for A) and a perturbation of a solitary wave (with the plus sign for A). If one adds an arbitrary constant to the expression (3.9) for B, it will still be a solution of (2.2). Figure 1 shows the bifurcation diagram for both the sech^2 and sech^4 bumps.

In order to integrate numerically the fKdV equation, we used the Fourier spectral method briefly described in Appendix A.1. The partial differential equation is solved on a periodic domain. We performed the following numerical computations. First we tested the exact solution. By inserting the exact solution for η in the time-dependent code, we checked that the solution does not change. Then we started with a flat free surface ($\eta = 0$), for various values of the Froude number larger than $F_{\min}$. The numerical solution always converged after some time to the stationary solution with the minus sign for A. Finally, we perturbed the stationary solutions by multiplying them by a factor smaller or greater than one.

The stability of the flow past an obstacle in either form of (3.11) has already been studied by Camassa and Wu [8,9], both analytically and numerically. They used the Hessian of the Hamiltonian (2.4) and perturbative methods in order to reach conclusions on the stability. We briefly recall these results in our set of parameters (the stability results are indicated as well in Fig. 1).

In the case of the sech^2-type obstacle, the perturbed solitary-wave solution with $A = F - 1 + \sqrt{(F-1)^2 - G}$ is always unstable. In contrast, the perturbed uniform flow solution $A = F - 1 - \sqrt{(F-1)^2 - G}$ is stable if and only if $G \leq \frac{80}{81}(F-1)^2$.

In the case of the sech^4-type obstacle, the perturbed solitary-wave solution with $A = F-1+\sqrt{(F-1)^2 - 2G/3}$ is unstable whereas the perturbed uniform flow solution $A = F - 1 - \sqrt{(F-1)^2 - 2G/3}$ is stable.

Numerical results are given for a sech^2-type obstacle in Fig. 2 (perturbed uniform flow) and in Fig. 3 (perturbed solitary wave). The perturbed uniform stream is stable in the sense that, when it is slightly perturbed, the numerical results show evidence of the tendency of the system to recover the stationary state (the decrease in amplitude of the wave on the right of Fig. 2 is real, even if it cannot be seen clearly on the figure). The perturbed solitary wave is unstable. With a perturbed initial condition which is smaller than the stationary solution, the solitary wave decreases in amplitude and goes directly towards the perturbed uniform stream. With a perturbed initial condition which is larger than the stationary solution, a large solitary wave is generated and propagates to the left (upstream), leaving behind a small stationary wave, which is the perturbed uniform stream. This is the well-known generation of upstream advancing solitons by moving disturbances explained by Ertekin et al. [26] and Wu [6]. A full account of numerical results with the same type of initial conditions can be found in [8]. The main purpose of this section was to check that our numerical code reproduces earlier results.
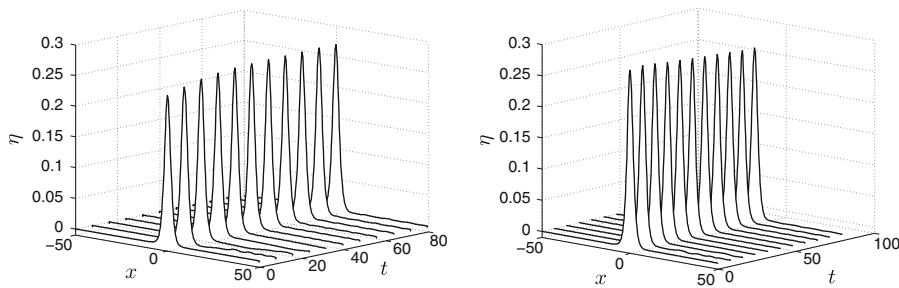
Fig. 2 Evolution of the stable perturbed uniform flow solution when $F = 1.32$ and $G = 0.1$, with a sech²-type obstacle. The initial condition is the exact solution times 0.9 (*left*) and 1.05 (*right*)
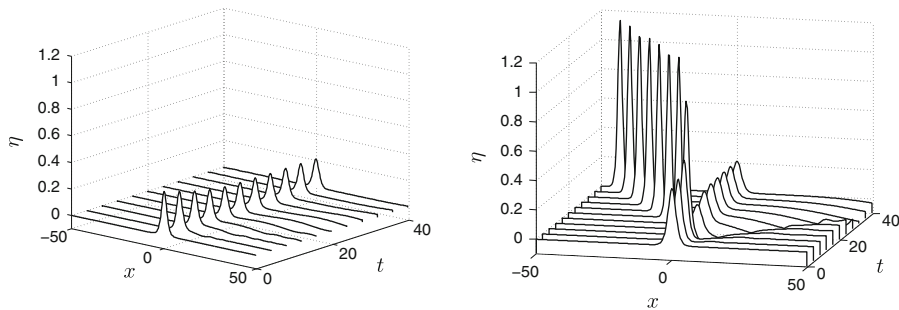

Fig. 3 Evolution of the unstable perturbed solitary-wave solution when $F = 1.32$ and $G = 0.1$, with a sech²-type obstacle. The initial condition is the exact solution times 0.9 (*left*) and 1.05 (*right*). In both cases the solution evolves toward the perturbed uniform stream above the bottom-mounted obstacle centred at $x = 0$

4 One obstacle: review of fronts and their stability

The topic of hydraulic falls is discussed in detail in all classical books on hydraulics. Hydraulic falls are generated by an obstacle. They connect a subcritical uniform flow with a supercritical uniform flow. They are only observed with subcritical flow upstream, as described for example in the monograph by Viollet et al. [27, pp. 337–338]. Forbes [28] investigated hydraulic falls experimentally, and he and others, including the authors themselves, computed hydraulic falls by solving the full Euler equations [29–32]. The stability of fronts has been less studied.[2] In order to investigate the stability of fronts, we first use the same inverse method as above to compute exact fronts, which connect two different uniform flows upstream and downstream of the obstacle. Assume that the front at the surface of the channel is of the form

$$\eta = A\left(1 + \tanh \beta x\right), \quad \beta \neq 0. \tag{4.1}$$

It is a rising front if $\beta > 0$ and a falling front if $\beta < 0$. We look for a corresponding bump at the bottom. In order to do this, we substitute (4.1) in (2.2). Again, after integration, one obtains (3.8). We do not write explicitly the expression for $B(x)$ but we impose that $B \to 0$ at $\pm\infty$. It leads to

$$A = \frac{2}{3}(F - 1).$$

Note that the resulting shape of the obstacle is not symmetric. One has a one-parameter family of such exact fronts,

$$\eta = \frac{2}{3}(F - 1)\left(1 + \tanh \beta x\right), \tag{4.2}$$

---

[2] One of the reviewers brought to our attention the recent paper by Donahue and Shen [15], where a stability analysis of fronts is performed in the same spirit as in the present paper. Our results are in perfect agreement.
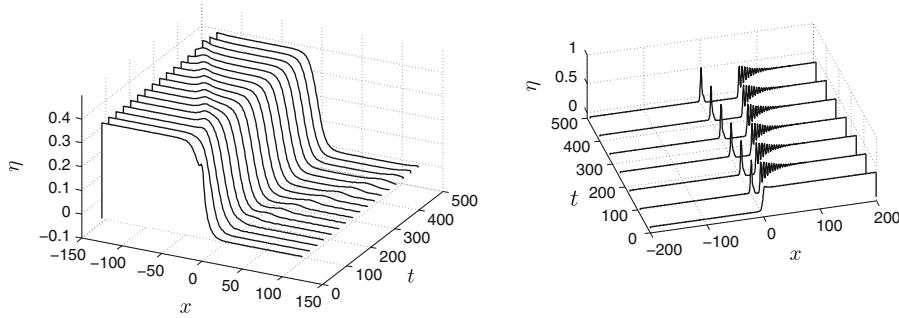
Fig. 4 *Left* Falling front (4.2) for $F = 1.3$ and $\beta = -0.1$. The front is stable. *Right* Rising front (4.2) for $F = 1.3$ and $\beta = 0.5$. The front is unstable. The initial condition is the exact solution plus $0.1 \operatorname{sech}(0.5\,x)$

for a given Froude number. This implies that the flow is subcritical on the top part of the solution and supercritical on the bottom part of the solution.

One also has

$$B(0) = 2(F-1)\frac{2}{3}(F-1) - \frac{3}{2}\frac{4}{9}(F-1)^2 = \frac{2}{3}(F-1)^2.$$

If β tends to zero, then η_{xx} converges uniformly to zero and $\frac{2}{3}(F-1)^2$ is the maximal height of the obstacle. It is also worth noticing that, if we had replaced the hyperbolic tangent by another smooth function with the same limits at $+\infty$ and $-\infty$ and a bounded second derivative, the maximal height would have also converged to $\frac{2}{3}(F-1)^2$ when $\beta \to 0$.

Numerically, the case of fronts is harder to handle since periodic boundary conditions cannot be used. The numerical scheme that we used is described in Appendix A.2. We found that the falling front is stable as shown on Fig. 4. Donahue and Shen [15] perturbed the falling front with white-noise and reached the same conclusion. As one can see on the right part of Fig. 4, the rising front is much less robust than the falling one, thus explaining why only falling fronts are observed in nature. The rising front becomes localized above the bottom-mounted obstacle. However, it is difficult to draw general conclusions on the stability since the boundary conditions play an important role in the evolution of the front.

5 Two obstacles: exact localised solutions with two humps and their stability

Supercritical flows over two obstacles on a channel bottom were considered both by Gong and Shen [10] and Binder et al. [14]. Gong and Shen [10] only considered the fKdV model and Binder et al. [14] calculated fully nonlinear solutions by a boundary-integral-equation method in addition to deriving weakly nonlinear solutions. Classical solutions were recovered and new solutions were found. In this paper, we investigate the stability of only two types of solutions: solutions with two humps above the two bottom-mounted obstacles in this section and table-top solutions in the next section.

In this section we assume that the solitary wave at the surface of the channel is of the form

$$\eta(x) = A_1 \operatorname{sech}^2 \beta_1 (x - x_1) + A_2 \operatorname{sech}^2 \beta_2 (x - x_2), \tag{5.3}$$

that is, the superposition of two solitary waves $\eta_1(x)$ and $\eta_2(x)$ centred at $x = x_1$ and at $x = x_2$, respectively. We look for a corresponding double bump at the bottom. In order to do this, we insert (5.3) into (2.2). Again, after integration, one obtains (3.8). The expression for $B(x)$ can be written explicitly as

$$B(x) = B_1(x) + B_2(x) - B_{12}(x), \tag{5.4}$$

where $B_1(x)$ and $B_2(x)$ are given by (3.9), with x replaced, respectively, by $x - x_1$ and $x - x_2$. The term $B_{12}(x)$ is equal to
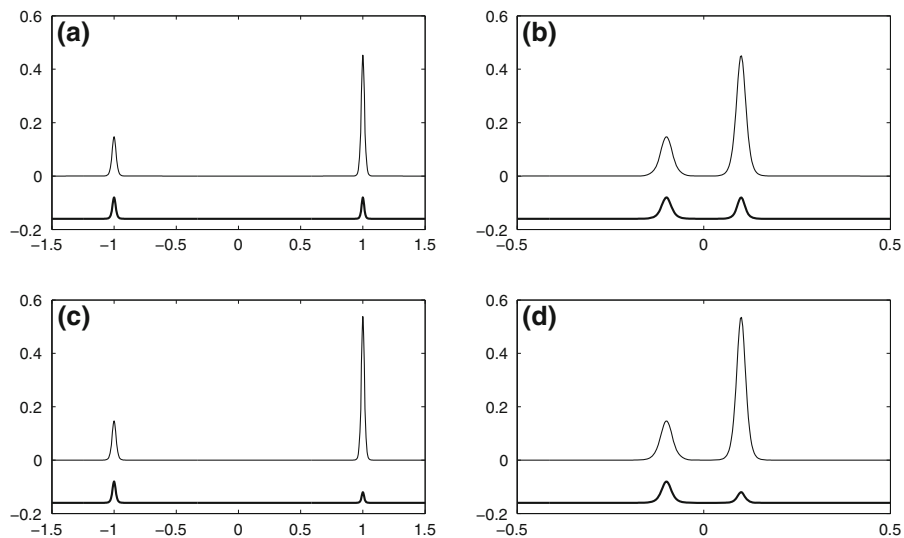
$$B_{12}(x) = 3\eta_1(x)\eta_2(x).$$

Fig. 5 Exact solutions (5.3) for a channel bottom with two bumps. **a** Same-size obstacles, with a perturbation on a uniform flow and a perturbation on a solitary wave; **b** same as (**a**) with the obstacles closer; **c** same as (**a**) with different size obstacles; **d** same as (**c**) with the obstacles closer
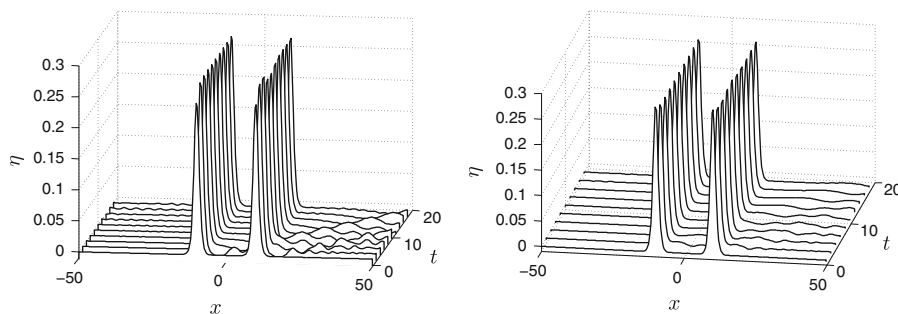

Fig. 6 Evolution of the perturbed uniform flow solution $\eta(x, t)$ when $F = 1.5$, $x_2 - x_1 = 20$, $G = 0.3$, with two sech^4-type obstacles. The initial condition is the exact solution times 0.9 (*left*) and 1.05 (*right*)

If the separation between the two bumps is sufficiently large, this term is extremely small. So, as a first approximation, one could for given values of F, G_1 (size of the first obstacle) and G_2 (size of the second obstacle) find the corresponding values of A_1, β_1 for the first obstacle and A_2, β_2 for the second obstacle as if there were no interaction between them. But it turns out that we can use this inverse method for constructing exact solutions, even if the two obstacles are not that far from each other. We now summarize the method for constructing bottoms with two bumps for which we know exact solutions. Choose F, G_1 and G_2. Then compute A_1, β_1 and A_2, β_2 from one of the two formulas (3.11). Four examples are shown in Fig. 5: two with obstacles of the same size and two with obstacles of different sizes.

Having these exact solutions, we then study their stability numerically. We follow the same approach as in the previous section: we perturb the stationary solutions by multiplying them by a factor smaller or greater than one. Like in the single-obstacle case, the perturbed uniform flow is stable, as long as the two obstacles are not too close: when it is slightly perturbed, the numerical results show evidence of the tendency of the system to recover the stationary state as shown on Fig. 6.

Next we consider the stability of the perturbed solitary-wave solution. Like in the single-obstacle case, the perturbed solitary wave is unstable. This can be seen on Fig. 7. With a perturbed initial condition which is smaller than the stationary solution, the solitary waves decrease in amplitude and go directly towards the perturbed uniform
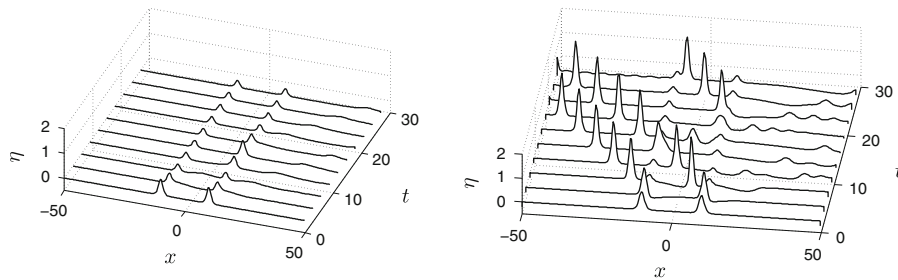
Fig. 7 Evolution of the perturbed solitary-wave solution $\eta(x, t)$ when $F = 1.5$, $x_2 - x_1 = 20$, $G = 0.3$, with two sech^4-type obstacles. The initial condition is the exact solution times 0.9 (*left*) and 1.05 (*right*). In both cases the solution evolves toward the perturbed two-hump uniform stream above the two bottom-mounted obstacles
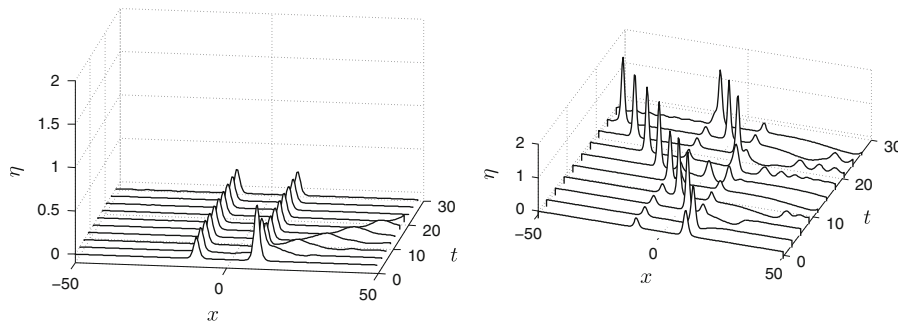

Fig. 8 Evolution of the solution which is a 'perturbed' uniform flow on the left-hand side and a perturbed solitary wave on the right-hand side when $F = 1.5$, $x_2 - x_1 = 20$, $G = 0.3$, with two sech^4-type obstacles. The initial condition is the exact solution times 0.9 and 1.05, respectively

stream, even if the disturbance moving to the right temporarily perturbs the signal above the right bump. With a perturbed initial condition which is larger than the stationary solution, solitary waves are generated by the moving disturbances and propagate upstream, leaving behind a small two-hump stationary wave above the two bottom-mounted obstacles, which is the perturbed uniform stream.

Finally we consider the stability of the solution which is a perturbed uniform flow on one side and a perturbed solitary wave on the other side. These solutions are unstable. This can be seen on Fig. 8, where the perturbed uniform stream is on the left, and Fig. 9, where the perturbed uniform stream is on the right. In Fig. 8, with an initial condition smaller than the steady solution (left plot), nothing spectacular occurs: the perturbed uniform flow goes back to the stationary state and the perturbed solitary wave goes to the perturbed uniform flow. A small disturbance moves downstream. In Fig. 8, with an initial condition larger than the steady solution (right plot), the upstream advancing soliton generated above the right obstacle interacts with the perturbed uniform stream. A new disturbance then moves downstream and seems to excite a second upstream advancing soliton. In Fig. 9, with an initial condition smaller than the steady solution (left plot), the perturbed solitary wave goes to the perturbed uniform flow and the perturbed uniform flow goes back to the stationary state but it feels the influence of the disturbance originating above the left obstacle and moving downstream. In Fig. 9, with an initial condition larger than the steady solution (right plot), there is an upstream advancing soliton generated above the left obstacle. Otherwise, the perturbed uniform flow goes back to the stationary state and the perturbed solitary wave goes to the perturbed uniform flow.

6 Two obstacles: exact table-top solutions and their stability

In the previous section we considered solutions which were essentially localized solitary waves above each obstacle. Binder et al. [14] found many more solutions in the presence of two obstacles, in particular supercritical solutions
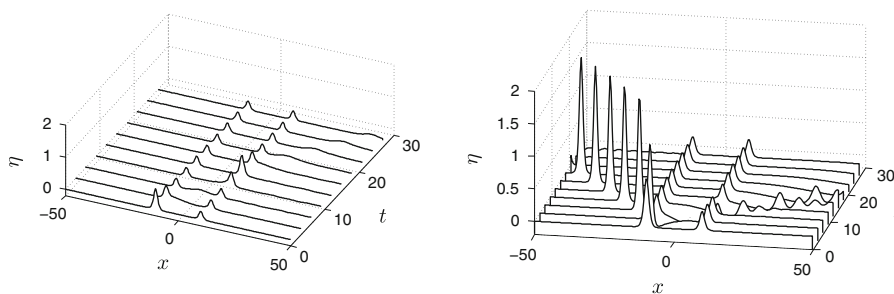
Fig. 9 Evolution of the solution which is a 'perturbed' solitary wave on the left-hand side and a perturbed uniform flow on the right-hand side when $F = 1.5$, $x_2 - x_1 = 20$, $G = 0.3$, with two sech^4-type obstacles. The initial condition is the exact solution times 0.9 and 1.05, respectively

with a train of waves trapped between the obstacles. The distance the obstacles are apart determines the number of waves trapped between the two obstacles. For the symmetric flows with two identical obstacles, solutions can be viewed as a matching of a generalised hydraulic rise over a single obstacle with a generalised hydraulic fall over a single obstacle. It turns out that these trapped waves can be eliminated midstream by satisfying a condition on the Froude number. For the full Euler equations, this condition was derived by Binder et al. [14] by using the conservation of mass and the dynamic boundary condition. These waveless solutions depend on one less parameter and either the Froude number or the obstacles height comes as part of the solution.

In the context of the fKdV equation, we assume now that the free surface is of the form depicted on Fig. 10:

$$\eta_{\beta,L} = A\tanh\beta(x - L) - A\tanh\beta(x + L), \quad A = \frac{2}{3}(F - 1). \tag{6.1}$$

In other words, it is the superposition of two fronts centred at $x = L$ (rising front) and at $x = -L$ (falling front), where L is a positive parameter and β negative. We look for a corresponding double bump at the bottom. In order to do this, we substitute (6.1) in (2.2). Again, after integration, one obtains (3.8). The bottom, which is symmetric, is denoted by $B_{\beta,L}$. However, each "individual" obstacle is not symmetric. The value of L must be large enough to allow for two separate bumps at the bottom and a real table-top free-surface profile.

Next we investigate the stability of these solutions. In addition to the numerical results, we first provide some analytical results on the stability. These results are only partial: indeed, they do not provide stability or instability for all cases. More details can be found again in [25]. First we study the spectrum of the Hessian of the Hamiltonian (2.4) with the help of Sturm–Liouville theory. We assume that $\beta < 0$ and $L > 0$. One is interested in the eigenvalues of the Hessian $\mathcal{L}$ of the Hamiltonian near $\eta = \eta_{\beta,L}$ when $B = B_{\beta,L}$.

The essential spectrum of $\mathcal{L}$ is $\sigma(\mathcal{L}) = [2(F - 1), +\infty[$ and 0 does not belong to it. Let $n_+(\beta, L)$ be the number of strictly positive eigenvalues of $\mathcal{L}_{\beta,L}$. Chardard [25] showed that the number $n_+(\beta, L)$ can jump by at most one as β and L vary continuously.

If β and x are fixed, then $\eta_{\beta,L}(x)$ is an increasing function of L and

$$L_1 < L_2 \Rightarrow \forall u \quad \langle u, \mathcal{L}_{\beta,L_1}u \rangle \leq \langle u, \mathcal{L}_{\beta,L_2}u \rangle.$$

Consequently, $n_+(\beta, L)$ is an increasing function of L when β is fixed. When $L = 0$, $\eta = 0$ and therefore $n_+(\beta, 0) = 0$. It follows that there exists a sequence $L_i(\beta)$, $0 < L_1(\beta) < L_2(\beta) < \ldots$, such that $n_+(\beta, L) = i$ if and only if $L \in]L_i(\beta), L_{i+1}(\beta)]$, e.g.

$$n_+(\beta, L) = \sum_{i=1}^{+\infty} \mathbb{1}_{]L_i(\beta),+\infty[}(L).$$

We provide some estimates of $L_i(\beta)$ when $F = 1.2$ and $\beta = -0.3$ in Table 1. One can also find an analytical estimate of $L_{i+1}(\beta) - L_i(\beta)$. Let $\zeta_{\beta,L}$ be a solution of system (2.5) when $\lambda = 0$ such that
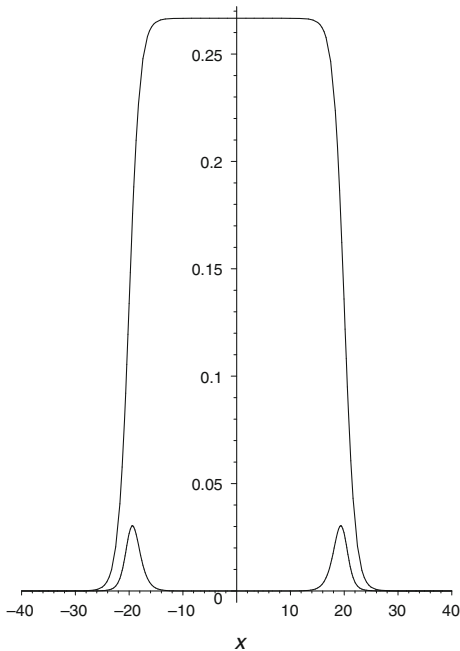
$$\lim_{x\to-\infty} \zeta_{\beta,L}(x) = 0.$$

Fig. 10 Table-top solution (6.1) past two obstacles when $L = 20$, $F = 1.2$ and $\beta = -0.5$
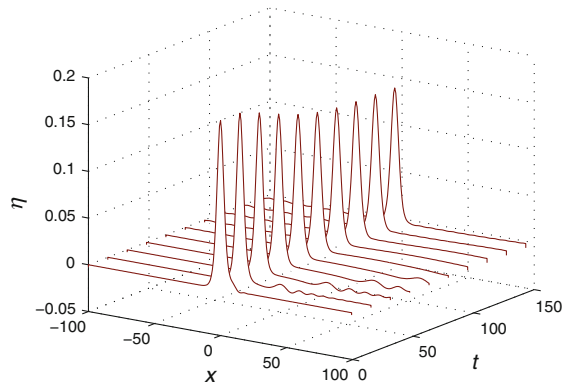

Fig. 11 Stable solution (6.1) when $L = 2$, $\beta = -0.3$ and $F = 1.2$ (In that case $n_+(-0.3, 2) = 0$). The initial condition was a perturbation of the stable solution

Table 1 Estimates of $L_i(\beta)$ when $F = 1.2$ and $\beta = -0.3$			
$L_1(-0.3)$	2.36823	$L_6(-0.3)$	9.32896
$L_2(-0.3)$	3.65133	$L_7(-0.3)$	10.7628
$L_3(-0.3)$	5.04097	$L_8(-0.3)$	12.1967
$L_4(-0.3)$	6.46378	$L_9(-0.3)$	13.6306
$L_5(-0.3)$	7.89555	$L_{10}(-0.3)$	15.0646

The number $n_+(\beta, L)$ is equal to twice the number of rotations of $\zeta_{\beta,L}$ around zero. If we set $\widetilde{\eta}_{\beta,\infty} = \frac{4}{3}(F - 1)$, then

$$\mathbf{C}_{\beta,\infty}(\lambda) = \begin{pmatrix} -6(F - 1) + 6\lambda & 0 \\ 0 & -1 \end{pmatrix},$$

which is approximately the value of $\mathbf{C}_{\beta,L}(x, \lambda)$ when x is close to 0. When $\lambda = 0$, the wavelength ℓ of the associated system is $2\pi/\sqrt{6(F - 1)}$ (0 is then in the essential spectrum). Therefore, when $2L$ increases by ℓ, the flat zone on which $\mathbf{C}_{\beta,L}(x, \lambda) \simeq \mathbf{C}_{\beta,\infty}(\lambda)$ also increases by ℓ. The number $n_+(\beta, L)$ should increase by approximately $\ell(2\sqrt{6(F - 1)})/\pi$. So one could expect that

$$L_{i+1}(\beta) - L_i(\beta) \sim_{i \to \infty} \frac{\pi}{2\sqrt{6(F - 1)}}.$$

For $F = 1.2$, the numerical value is 1.4339, which is consistent with Table 1.

We now use formula (2.6) for this particular solution. Recall that (2.6) states that

$$n_+(\beta, L) = N_{\text{unst}} + N_{\text{imag}}^+,$$

where N_{unst} is the number of unstable modes of $\partial_x \mathcal{L}_{\beta,L}$ and N_{imag}^+ is the number of oscillatory modes u of $\partial_x \mathcal{L}_{\beta,L}$ such that $\langle u, \mathcal{L}_{\beta,L} u \rangle > 0$. If $N_{\text{unst}} \neq 0$, the stationary solution is unstable. Otherwise, it is said to be spectrally stable. There are two cases for which it is possible to conclude on the stability of the table-top solutions:
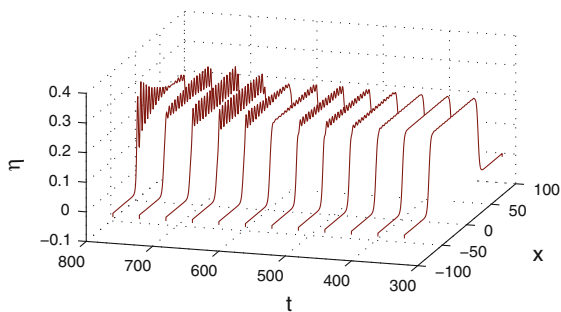
Fig. 12 Instability developing on the table-top solution (6.1) when $L = 50$, $\beta = -0.3$ and $F = 1.2$ (In that case $n_+(-0.3, 50) = 34$). The leading instability seems to be associated to a complex eigenvalue, since the instability has not a uniform growth rate (the instability appears alternatively on the right and the left of the table-top solution). There are 16 oscillations developing between the two edges of the solution, which is quite close to the 17 expected oscillations
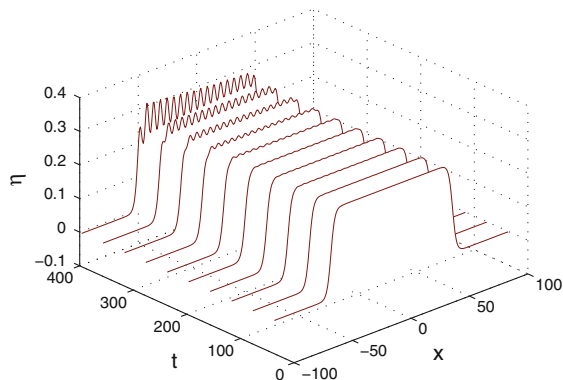
Fig. 13 Instability developing on the table-top solution (6.1) when $L = 52$, $\beta = -0.3$ and $F = 1.2$ (In that case $n_+(-0.3, 52) = 35$). Here, the leading instability seems to be associated to a real eigenvalue, since it grows rather uniformly. There are 17 oscillations developing between the two edges of the solution, which is quite close of the 18 expected oscillations

- $L \in [0, L_1(\beta)[$. The solution is stable (see Fig. 11). But then the solution is not really a table-top solution since the obstacles are not really separated.
- $L \in \cup_{i \in \mathbb{N}}]L_{2i+1}(\beta), L_{2i+2}(\beta)[$. The table-top solution is unstable.

In the first case, the lowest eigenvalue of $\mathcal{L}_{\beta,L}$ is strictly positive. Therefore $N_{\text{unst}} = 0$. From Sect. 5 of [8], this also implies the nonlinear stability of the stationary solution.

In the second case, $n_+(\beta, L)$ is an odd number and there is no zero eigenvalue. Since N_{imag}^- is even, N_{unst} is odd and hence non-zero. Therefore, the solution is unstable.

If $L \in \cup_{i \in \mathbb{N}}[L_{2i+2}(\beta), L_{2i+3}(\beta)]$, none of the previous arguments works. However, numerical simulations seem to indicate that these solutions are also unstable.

We tried to determine the stability of table-top solutions by integrating numerically the fKdV system. Except for $L \in [0, L_1(\beta)[$, all the table-top solutions we observed were unstable, although some instabilities were slower to appear than others. In fact, there were two kinds of leading instabilities:

- Some oscillations increased alternatively in the left and in the right of the table-top part of the solution. This seems to indicate a leading pair of complex eigenvalues (see Fig. 12). Note that time starts at $t = 300$ in the figure, since nothing happens before.
- Some oscillations grew rather uniformly on the table-top part of the solution. This seems to indicate a leading real eigenvalue (see Fig. 13).

In both cases, the oscillations eventually grew to the point of escaping from the trap.

We observed that the period of the oscillations appearing in the table-top part of the solution could be accurately predicted by the dispersion relation of the system when $\eta = \eta_{\beta,\infty} = \frac{4}{3}(F - 1)$. The dispersion relation for $\eta = \eta_{\beta,\infty} = \frac{4}{3}(F - 1)$ is indeed

$$\omega = k\left(\frac{k^2}{6} - (F - 1)\right).$$

If one looks for stationary oscillations, then $\omega = 0$. This implies $k = 0$ or $k = \sqrt{6(F - 1)}$, so that the wavelength of the oscillation is $2\pi/\sqrt{6(F - 1)}$. As a consequence, one could expect roughly $L\sqrt{6(F - 1)}/\pi$ oscillations developing between the obstacles and these oscillations were indeed observed.

7 Conclusion and discussion

While there have been several papers devoted to the stability of solutions of the fKdV equation when the forcing is a single obstacle, there have been many fewer studies on multiple forcing. After reviewing briefly the stability results for localized solutions above a single obstacle and the much more recent stability results for fronts, we have concentrated on the stability of flows past two obstacles. Rather than computing numerical solutions of the stationary fKdV equation, we have used the inverse method to construct channel bottoms providing exact expressions for the free-surface deformation. Two types of free surfaces have been considered: free surfaces with two localised humps above the two bottom-mounted obstacles and table-top free surfaces. We have numerically demonstrated the stability of solutions with two localised humps which are perturbed uniform streams. We have analytically (partially) and numerically demonstrated the instability of table-top solutions.

The main motivation to introduce two obstacles was to try to generate the generalised critical flows first calculated by Dias and Vanden-Broeck [12]. These generalised critical flows lack physical meaning because the waves do not satisfy the radiation condition which requires that there be no energy coming from infinity. However Dias and Vanden-Broeck [13] showed that the radiation condition can be satisfied by introducing a second obstacle in the channel. The waves can then be trapped between the two obstacles. The present results seem to indicate that these solutions are unstable.

Binder et al. [14,33] considered various kinds of forcings, including two bumps and a step. A plethora of surface-wave profiles were found. There are a lot of stationary free-surface profiles for which the stability has not been investigated yet. Flows in which the disturbance lies on the free surface are also interesting. Binder and Vanden-Broeck [34] showed that there are no subcritical or critical solutions satisfying the radiation condition for steady flows past a flat plate. Binder et al. [35] used a weakly nonlinear theory to show that solutions for subcritical and critical flows can be constructed provided the flat plate is replaced by a curved plate. Again no stability studies of these solutions have been performed yet.

We conclude by stating that a rigorous analytical proof of the stability or instability of all the known stationary profiles of the fKdV model is yet to be provided.

Appendix: Details about the numerical simulations

Two methods have been used for the various numerical simulations: a Fourier spectral method for all the cases where the solution goes to zero both at plus and minus infinity (the periodicity required by the spectral method is then satisfied), and a finite-difference scheme to compute the fronts in Sect. 4 (the periodicity condition is no longer satisfied). Note that Donahue and Shen [15] used a different method to compute fronts: they treated fronts as phenomena observed near the bump. They overcame the difficulty associated with the non-periodicity by using a very large value for the end of the domain (say $x = W$) and letting the stationary solution extend only to $\pm(1/2)W$. Hence the end conditions at $x = \pm W$ are still zero. Of course, a discontinuity is introduced but it was found that the resulting disturbance did not affect the solution in the vicinity of the bump.

A.1. Simulation on a periodic domain

Suppose that x takes values in the interval $[-W \ \ W]$.[3] In order to work in the interval $[-\pi \ \ \pi]$, we use the scaling coefficient $S = \pi/W$:

$$Sx = x_{\text{new}}, \quad x_{\text{new}} \in [-\pi \ \ \pi].$$

Equation (2.2) becomes

$$\eta_t = \frac{1}{6} S^3 \eta_{xxx} + \frac{3}{4} S \left(\eta^2 \right)_x - (F - 1) S \eta_x + \frac{1}{2} S B_x, \tag{A.1}$$

where the same notation has been kept for the sake of simplicity.

---

[3] Even though solutions are computed in the interval $[-W \ \ W]$, they are not necessarily shown on the entire interval in the figures

The numerical integration is performed by using a Fourier spectral method. The fKdV equation is then discretized in space by using the following grid with $2J$-points:

$$(\eta_t)_j = \left(\frac{1}{6}S^3 D^3 \eta + \frac{3}{4} SD\left(\eta^2\right) - (F-1)SD\eta + \frac{1}{2}SB_x\right)_j, \quad j = 1, \ldots, 2J \qquad (A.2)$$

where D is the spectral derivative. Recall that the operator D acts as follows:

$$\left(\widehat{Du}\right)_r = \mathrm{i}r\widehat{u}_r \quad \text{for} \quad -J+1 \leq r \leq J-1, \qquad (A.3)$$

where $\widehat{}$ denotes the Discrete Fourier Transform.

Equation (A.2) is then discretized in time by using the explicit fourth-order Runge–Kutta method.

A.2. Simulation on a finite interval

For the front solutions, it is difficult to use periodic boundary conditions. So we used a finite difference scheme with the following boundary conditions:

$$u_x(-W, t) = u_{xx}(-W, t) = 0, \quad u(W, t) = 0. \qquad (A.4)$$

In [36], it is proved that the Korteweg–de Vries equation subject to these boundary conditions is locally well-posed as long as the initial data also satisfies these boundary conditions. Colin and Gisclon [36] also provided a semi-implicit finite difference scheme of order one which we adapted to the fKdV equation:

$$\left(u^{n+1} - \frac{1}{6}D^- D^- D^+ u^{n+1} - u^n - \Delta t\left(\left(\frac{3}{2}u^n + (F-1)\right)D^+ u^n - B_x\right)\right)_j = 0$$

when $j \in \{3, \ldots, J-1\}$. The superscripts refer to time discretization and D^+ and D^- denote, respectively,

$$(D^+ v)_j = \frac{v_{j+1} - v_j}{\Delta x}, \qquad (D^- v)_j = \frac{v_j - v_{j-1}}{\Delta x}.$$

The boundary conditions are discretized by:

$$u_1 = u_2 = u_3, \qquad u_J = 0.$$

The obvious drawbacks of this approach are that spectral precision is lost and a linear inversion is necessary. If one wants to use another value than 0 for $u(W, t)$ on the right, especially in the case of a rising front, one can make the following change of variable: $u \to u + C$ and $F \to F - \frac{2}{3}C$.

Note that Higgins et al. [37] have introduced an efficient series-solution method for free-boundary problems arising from flow over topography.

References

1. Baines PG (1995) Topographic effects in stratified flows. Cambridge University Press, New York
2. Akylas TR (1984) On the excitation of long nonlinear water waves by a moving pressure distribution. J Fluid Mech 141:455–466
3. Grimshaw RH, Smyth N (1986) Resonant flow of a stratified fluid over topography. J Fluid Mech 169:429–464
4. Patoine A, Warn T (1982) The interaction of long, quasi-stationary baroclinic waves with topography. J Atmos Sci 39:1019–1025
5. Pratt LJ (1984) On nonlinear flow with multiple obstructions. J Atmos Sci 41:1214–1225
6. Wu TY (1987) Generation of upstream advancing solitons by moving disturbances. J Fluid Mech 184:75–99
7. Shen SSP (1991) Locally forced critical surface waves in channels of arbitrary cross section. J Appl Math Phys (ZAMP) 42:122–138
8. Camassa R, Wu TY (1991) Stability of forced steady solitary waves. Philos Trans R Soc Lond A 337:429–466
9. Camassa R, Wu TY (1991) Stability of some stationary solutions for the forced KdV equation. Physica D 51:295–307
10. Gong L, Shen SSP (1994) Multiple supercritical solitary wave solutions of the stationary forced Korteweg–de Vries equation and their stability. SIAM J Appl Math 54:1268–1290
11. Shen SSP, Shen B, Ong CT, Xu ZT (2002) Collision of uniform soliton trains in asymmetric systems. Dyn Contin Discr Impuls Syst B9:131–138

12. Dias F, Vanden-Broeck J-M (2002) Generalised critical free surface flows. J Eng Math 42:291–301
13. Dias F, Vanden-Broeck J-M (2004) Trapped waves between submerged obstacles. J Fluid Mech 509:93–102
14. Binder BJ, Vanden-Broeck J-M, Dias F (2005) Forced solitary waves and fronts past submerged obstacles. Chaos 15:037106-1–037106-13
15. Donahue AS, Shen SSP (2010) Stability of hydraulic fall and sub-critical cnoidal waves in water flows over a bump. J Eng Math 68:197–205
16. Maleewong M, Asavanant J, Grimshaw R (2005) Free surface flow under gravity and surface tension due to an applied pressure distribution: I Bond number greater than one-third. Theor Comput Fluid Dyn 19:237–252
17. Grimshaw R, Maleewong M, Asavanant J (2009) Stability of gravity-capillary waves generated by a moving pressure disturbance in water of finite depth. Phys Fluids 21:082101
18. Sautreaux C (1901) Mouvement d'un liquide parfait soumis à la pesanteur. Détermination des lignes de courant. J Math Pures Appl 7:125–159
19. Wehausen JV, Laitone WV (1960) Surface waves. In: Flügge S (ed) Handbuch der Physik, vol 9. Springer, Heidelberg pp 446–778
20. Tuck EO, Roberts AJ (1997) Bow-like free surfaces under gravity. Philos Trans R Soc Lond A 355:665–677
21. Lee S, Yates G, Wu TY (1989) Experiments and analyses of upstream-advancing solitary waves generated by moving disturbances. J Fluid Mech 199:569–593
22. Shen SSP (1992) Forced solitary waves and hydraulic falls in two-layer flows. J Fluid Mech 234:583–612
23. Shen SSP (1995) On the accuracy of the stationary forced Korteweg–de Vries equation as a model equation for flows over a bump. Q Appl Math 53:701–719
24. Chugunova M, Pelinovsky D (2010) Count of eigenvalues in the generalized eigenvalue problem. J Math Phys 51:052901
25. Chardard F (2009) Stabilité des Ondes Solitaires. PhD thesis, Ecole Normale Supérieure de Cachan, France. http://tel.archives-ouvertes.fr/tel-00426266/en/
26. Ertekin RC, Webster WC, Wehausen JV (1986) Waves caused by a moving disturbance in a shallow channel of finite width. J Fluid Mech 169:275–292
27. Viollet P-L, Chabard J-P, Esposito P, Laurence D (1998) Mécanique des Fluides Appliquée. Presses de l'Ecole Nationale des Ponts et Chaussées, Paris
28. Forbes L (1988) Critical free-surface flow over a semi-circular obstruction. J Eng Math 22:3–13
29. Vanden-Broeck J-M (1987) Free-surface flow over an obstruction in a channel. Phys Fluids 30:2315–2317
30. Forbes LK, Schwartz LW (1982) Free-surface flow over a semicircular obstruction. J Fluid Mech 114:299–314
31. Dias F, Vanden-Broeck J-M (1989) Open channel flows with submerged obstructions. J Fluid Mech 206:155–170
32. Dias F, Vanden-Broeck J-M (2004) Two-layer hydraulic falls over an obstacle. Eur J Mech B 23:879–898
33. Binder BJ, Dias F, Vanden-Broeck J-M (2008) Influence of rapid changes in a channel bottom on free-surface flows. IMA J Appl Math 73:254–273
34. Binder BJ, Vanden-Broeck J-M (2005) Free surface flows past surfboards and sluice gates. Eur J Appl Math 16:601–619
35. Binder BJ, Vanden-Broeck J-M, Dias F (2009) On satisfying the radiation condition in free-surface flows. J Fluid Mech 624:179–189
36. Colin T, Gisclon M (2001) An initial-boundary-value problem that approximate the quarter-plane problem for the Korteweg–de Vries equation. Nonlin Anal 46:869–892
37. Higgins PJ, Read WW, Belward SR (2006) A series-solution method for free-boundary problems arising from flow over topography. J Eng Math 54:345–358